

> REPLACE THIS LINE WITH YOUR MANUSCRIPT ID NUMBER (DOUBLE-CLICK HERE TO EDIT) <

220-325-GHz Horn-type Adapter for Terahertz Microstructured Fiber Measurements

Rungrat Viratikul, Binbin Hong, Panuwat Janpugdee, Joachim Oberhammer, *Senior Member, IEEE*, Ian Robertson, *Fellow, IEEE*, Nutapong Somjit, *Senior Member, IEEE*

Abstract—In this paper, a novel and innovative approach to characterize THz Bragg fibers using a horn-type adapter is presented, enabling a two-tier calibration method for a direct, efficient, and reliable way to measure THz Bragg fibers, including return loss and insertion loss. The proposed approach is robust, accurate, and repeatable, making it suitable for designing and optimizing THz Bragg fibers and systems and enabling continued research and development. The present study employs a calibration approach, utilizing Short-Short-Load-Thru (SSLT) and Thru-Reflect-Line (TRL) calibrations. The horn-type adapter connects a standard WR-3.4 rectangular waveguide and a THz Bragg fiber, allowing the mode conversion from the TE_{10} mode in the rectangular waveguide to the HE_{11} mode in the Bragg fiber, with a middle stage of the TE_{11} mode in the tapered horn region. Additionally, the highly accurate measurement quality presented advantages compared to the existing THz measurement setups, for example, setup complexity, coupling efficiency, impedance adjustability, and less sensitivity to measurement environments, etc. The present approach shows advantages in experimental setup complexity, coupling efficiency, impedance adjustability, measurement repeatability, operator experience required, and setup tool cost compared to other existing THz measurement techniques.

Index Terms— THz microstructured fiber measurements, two-tier calibration, Horn-type adapter

This work was supported in part by the National Natural Science Foundation of China under Grant 62105213, in part by the Guangdong Basic and Applied Basic Research Fund under Grant 2020A1515111037, in part by Ph.D. Matching Fund granted by Electrical Engineering Department, Chulalongkorn University, in part by the Engineering and Physical Science Research Council under Grant EP/S016813/1 and in part by the Swedish Research Council (VR) under Grant 2021-05842_VR. (*Corresponding author: Nutapong Somjit.*)

B. Hong is with the Faculty of Arts and Sciences, Beijing Normal University, Zhuhai 519085, China. (e-mail: b.hong@bnu.edu.cn)

Rungrat Viratikul is with the Department of Electrical Engineering, Faculty of Engineering, Chulalongkorn University, Bangkok 10330, Thailand. (e-mail: 6571022121@student.chula.ac.th)

Panuwat Janpugdee is with the Department of Electrical Engineering and the Wireless Network and Future Internet Research Unit, Chulalongkorn University, Bangkok 10330, Thailand. (e-mail: Panuwat.Ja@chula.ac.th)

Joachim Oberhammer and Nutapong Somjit are with the Division of Micro and Nanosystems (MST), KTH Royal Institute of Technology, Malvinas väg 10, SE-100, Stockholm, Sweden (emails: joachimo@kth.se; somjit@kth.se)

Ian Robertson and Nutapong Somjit are with the School of Electronic and Electrical Engineering, University of Leeds, Leeds LS2 9JT, U.K. (e-mails: i.d.robertson@leeds.ac.uk; n.somjit@leeds.ac.uk)

Nutapong Somjit is with the Department of Electrical Engineering, Faculty of Engineering, Chiang Mai University 239, Huay Kaew Road, Muang District, Chiang Mai Thailand, 50200 (e-mail: nutapong.somjit@cmu.ac.th)

I. INTRODUCTION

RECENTLY, the most widely accepted definition of the THz band is that it extends from approximately 10 THz to 100 GHz (0.03-3.00 mm in wavelength) and is located between the microwave and infrared (IR) frequency bands [1]–[3]. Terahertz technology advancements and growing interest in applications have increased the demand for developing new sources [4]–[8], detectors, waveguides, and other components for efficient terahertz wave control [9]. However, high frequency, especially in the terahertz band, suffers from high metal ohmic loss and dielectric material absorption [10], which means that the traditional waveguides and fibers are not appropriate for low-loss long-distance waveguiding of the THz wave. Therefore, new concepts have to be developed for low-loss THz waveguides and fibers [11]–[13].

THz microstructured fibers [14], [15], i.e. the waveguides with artificially designed sub-wavelength microstructured transverse cross-sections, have attracted the interest of researchers due to their exceptional optical properties, which provide a versatile platform for tailoring the effective mode area and dispersion characteristics to suit various linear and nonlinear applications over wide bandwidths. An efficient coupling structure supporting quasi-single-mode propagation is needed, as unwanted multimode interference causes higher insertion loss and measurement complications. Single-mode operation is also crucial for many applications [16], and the design of a Bragg fiber that can provide low-loss, medium-range, and flexible solutions for interconnecting different functional components in THz communication, imaging, and sensing systems while also allowing for robust and repeatable characterization, is necessary. The development of THz measurement and characterization techniques require measurement accuracy, cost-effectiveness, and ease of setup. These properties are frequently influenced by the physical interaction between the device-under-test (DUT) and THz probes, and the design and optimization of such interactions are critical for achieving accurate and consistent measurements.

Contactless or free-space measurements [17], [18] are commonly used to characterize THz components and employ a variety of antennas, such as horn antennas [19]–[21], parabolic reflectors, and planar antennas, to transmit and guide THz test

> REPLACE THIS LINE WITH YOUR MANUSCRIPT ID NUMBER (DOUBLE-CLICK HERE TO EDIT) <

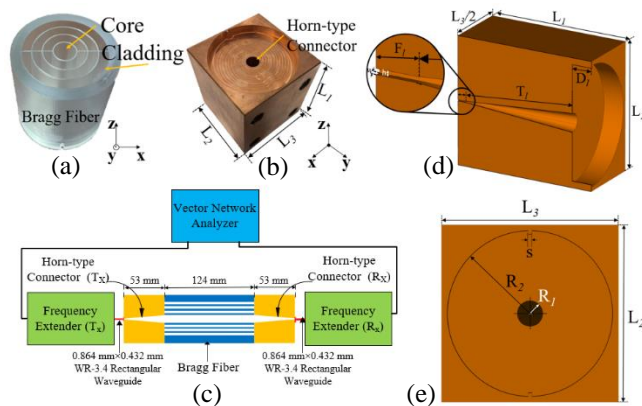


Fig. 1. The design and fabrication of a Bragg fiber and a Horn-type adapter used in this paper including the schematic of measurement setup. (a) Fabricated the designed Bragg fiber prototype using the Accura ClearVue used as DUT; (b) The horn-type adapter fabricated by CNC milling. (c) Illustration of electronic-based THz measurement setup using the HMRW-connector-Bragg fiber integrated system: the dimension of WR-3.4 is 0.864 mm×0.432 mm and the parameters of the Bragg fiber and the horn-type adapter are described in the Table I. (d) The schematic of the horn-type adapter including the dimension parameters. (e) Cross-sectional view of the horn-type adapter with the dimension parameters.

signals onto the input terminal of DUT and receive THz responses from its output. Furthermore, the free-space measurement technique overcomes many limitations of contact probe measurements, such as limited probe lifetime, mechanical and electrical degradation of the contact surface due to contact force, and fragility issues. On the other hand, contactless measurements are also sensitive to environmental conditions and alignment issues. Besides, contactless measurement setups require costly components such as parabolic mirrors, reflectors, and alignment units. THz microstructured fibers can also be an essential structure for designing functional devices, such as THz Bragg fiber filtering antennas, THz gas/liquid sensors [22], and THz endoscopy front-ends.

One method for THz-frequency measurements is waveguide-to-planar-probe measurements, which utilize rectangular waveguide flanges. These measurements can be performed using commercially available THz measurement extenders connected to a network analyzer, with options for different waveguide frequency bands up to 1.5 THz [23]. However, waveguide-to-planar-probe measurements, especially in THz bands, present contact resistance and other parasitic effects at the physical interface locations between the measurement probes and the DUT, substantially affecting the measurement integrity, accuracy, and reproducibility. Moreover, the operational life cycle of probes is also limited due to equipment durability. Apart from that, contact measurements are commonly used because of uncomplicated installations, better in repeatability and inexpensive compared to contactless measurements, which require some costly components and experienced technicians to construct and set up.

This paper proposes a robust, accurate, and repeatable characterization method of low-loss THz Bragg fibers [24] using a horn-type interface to connect to a standard rectangular waveguide and using a two-tier calibration technique [25]. The measurement setup is compact and straightforward, as it uses a horn-type adapter that directly interfaces with the THz Bragg fiber, eliminating the need for additional optical components and intricate alignment procedures. Furthermore, the two-tier calibration technique simplifies the calibration process and reduces the number of required calibration standards, making the setup less complex and more user-friendly than other THz measurement techniques. Compared to conventional THz measurement setups, the measurement system presented in this study allows for cost-effective and efficient customization to meet the measurement requirements. The setup can be easily customized to the needs of users, and the low-cost nature of the design makes it an attractive alternative to existing measurement techniques.

II. DESIGN OF THE HORN-TYPE ADAPTER

A horn-type adapter is a type of microwave connector with a flared shape, like a horn, which helps to reduce signal loss and improve the coupling efficiency between two interfaces. Fig. 1 (a) illustrates the device under test, which is a hollow Bragg fiber prototype using Accura ClearVue obtained from 3D Systems[®]. Fig. 1 (b) illustrates the proposed horn-type adapter fabricated by CNC milling.

The electronic-based THz measurement setup consists of the integration of Hollow Metallic Rectangular Waveguide (HMRW)-Horn-type adapter-Bragg fiber system, as depicted in Fig. 1 (c). Two high-frequency extenders with the operating band from 220 to 325 GHz are connected to a network analyzer to produce and analyze the THz test signal (T_x and R_x). The THz beam emitted from the horn antenna at the transmitting extender is fed into the input port of the DUT. It converts the dominant TE_{11} mode in the connector into the quasi HE_{11} mode in the Bragg fiber with low return loss. Fig. 1 (d) and (e) show the schematic and cross-sectional view of the copper horn-type adapter used in this measurement, and the designed geometric and optical parameters of the horn-type adapter are listed in Table I.

Fig. 2 (a) illustrates the cross-sectional view of THz hollow Bragg fiber and its geometrical parameters. The Bragg fiber consists of an air core with the refractive index ($n_c = 1$) surrounded by periodic concentric dielectric layers alternating between high (n_a) and low (n_b) refractive index materials with thicknesses of 0.64 and 3.88 mm., respectively.

> REPLACE THIS LINE WITH YOUR MANUSCRIPT ID NUMBER (DOUBLE-CLICK HERE TO EDIT) <

TABLE I

THE DESIGNED GEOMETRIC AND OPTICAL PARAMETERS OF HORN-TYPE ADAPTER AND BRAGG FIBER

Parameters	Description	Value
F_l	Flange length	3 mm
T_l	Tapered length	45.3 mm
D_l	The depth of cavity	5 mm
L_1, L_2 and L_3	The outmost dimensions of horn-type adapter	$53 \times 50 \times 50 \text{ mm}^3$
w	Width of Standard WR-3.4 RWG	0.864 mm
h	Height of Standard WR-3.4 RWG	0.432 mm
R_1	Radius of horn-type adapter	3.65 mm
R_2	Radius of Bragg fiber	23.25 mm
S	The edge to mount DUT with horn-type adapter	1 mm
σ	Electric Conductivity of horn-type adapter	$5.96 \times 10^7 \text{ S/m}$

The outermost layer has mechanical stability and resistance to environmental factors with a thickness of 4.6 and a width of support bridge of 0.65 mm., which are thick protective polymer layers and provide mechanical stability and resistance to environmental factors that absorb residual electromagnetic waves and isolate the fiber from outside interference. Fig. 2 (b) compares the dispersion curves of the HE_{11} mode of the Bragg fiber and the TE_{11} mode of the HMCW using the CST Simulation. The output face of a horn-type adapter can be characterized by its waist radius, which is the distance from the center of the face to the point where the Gaussian beam has its minimum radius. Fig 2 (c) and (d) show our measurement using terahertz time-domain spectroscopy, the refractive index and absorption coefficient of the Accura ClearVue between 0.2 – 1 THz can be fitted using $n = -0.0123f^2 - 0.0335f + 1.6262$, and $a(\text{cm}^{-1}) = 6.4667f^2 + 17.5066f - 2.0294$, respectively. Here, f is the frequency in THz unit.

This waist radius can be related to the core radius of a Bragg fiber through a parameter denoted as ρ . Different ratios of ρ can be used to optimize the coupling efficiency between the horn-type adapter and the Bragg fiber. Here, $\rho = r_0/r_c$, Where r_0 is the core radius of the horn-type adapter at the output face, and r_c is the core radius of the Bragg fiber. According to the momentum conservation principle, the phase velocity of the mode in the connector should be well matched to the phase velocity of the mode in the Bragg fiber to obtain the greatest transition between the horn-type adapter and the Bragg fiber.

As can be seen from the Fig. 2 (b), the dispersion curve of the HE_{11} mode of the Bragg fiber is overlapped with that of the TE_{11} mode of HMCW at around 0.27 THz when ρ is 0.77,

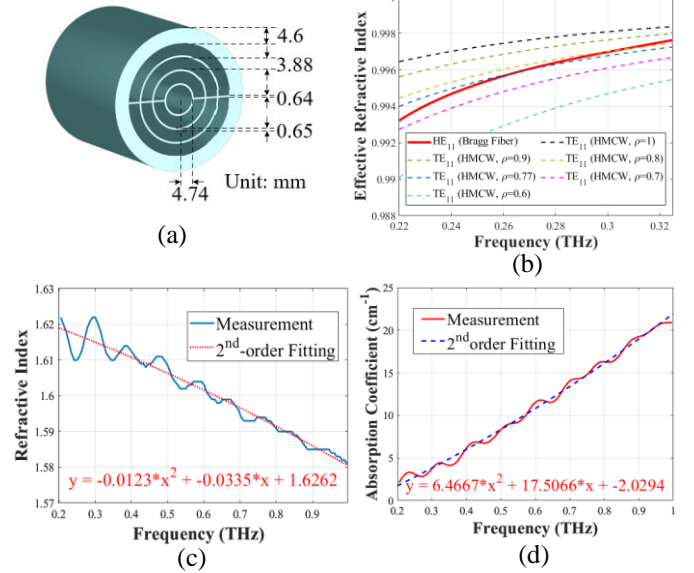


Fig. 2. The asymptotically single-mode hollow THz Bragg fiber used as DUT in this work, the relationship of impedance matching condition between the horn-type adapter and the Bragg fiber, and dielectric property of THz Bragg fiber using Accura ClearVue between 0.2 - 1 THz. (a) The geometrical structure and the cross-sectional view of THz hollow Bragg fiber, including its parameters. (b) The comparison of the dispersion curves of effective refractive index profile of the HE_{11} mode of the Bragg fiber and the TE_{11} mode of the HMCW with the different ratio of ρ using CST simulation. (c) Refractive index of Accura ClearVue. (d) absorption coefficient of Accura ClearVue.

which means their phase velocities are well matched, and hence offers the highest coupling efficiency. The input mode in [26] is a free-space Gaussian beam, while in this paper is a circular waveguide mode at the output aperture of the horn-type adapter. This mode is hybrid, with several competing modes present [27], but the main mode is the fundamental mode of hollow metallic circular waveguide (HMCW), namely the TE_{11} mode. The goal of phase matching is to minimize signal loss and reflection, ensuring that the maximum amount of electromagnetic energy is transferred from one waveguide to the other.

By achieving optimal phase matching, the electromagnetic energy can propagate efficiently from the horn-type adapter to the THz Bragg fiber, leading to more accurate and reliable measurements. The impedance values are measured experimentally using the vector network analyzer (VNA). The horn-type adapter is connected to a standard WR-3.4 waveguide and a Bragg fiber with an input aperture, which transfers the operating TE_{10} mode from the rectangular waveguide into the fundamental HE_{11} mode in the Bragg fiber, occurring as a linear polarization mode.

> REPLACE THIS LINE WITH YOUR MANUSCRIPT ID NUMBER (DOUBLE-CLICK HERE TO EDIT) <

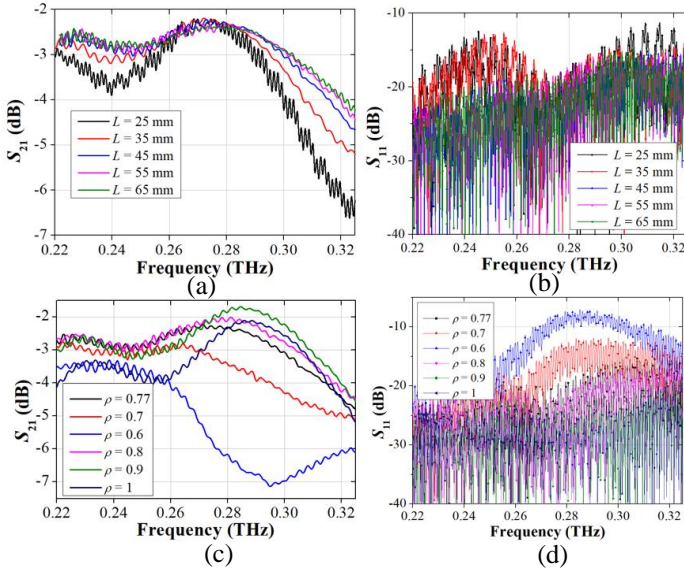


Fig. 3. The CST Simulation of the horn-type adapter using a back-to-back full simulation to compare the S_{11} and S_{21} with different taper lengths L and ρ . (a) the S_{21} by adjusting the taper length (L) between 25 – 65 mm and $\rho = 0.77$. (b) the S_{11} by adjusting the L between 25 – 65 mm and $\rho = 0.77$. (c) the S_{21} by adjusting the ρ between 0.6 – 1 and $L = 45$ mm. (d) the S_{11} by adjusting the ρ between 0.6 – 1 and $L = 45$ mm.

Fig. 3 shows the CST simulation results of a parametric study for the design of a horn-type adapter. Two design parameters which are the taper length L and the ratio ρ of the core radius of the horn-type adapter at the output face to the core radius of the Bragg fiber were investigated. The scattering parameters, S_{11} and S_{21} , were computed and compared for different values of L and ρ by varying one parameter at a time. Fig. 3 (a) and (b) show $|S_{21}|$ and $|S_{11}|$, respectively, for different values of L between 25 to 65 mm, and ρ is 0.77. The results show that the optimal value of L is 45 mm. On the other hand, Fig. 3 (c) and (d) show $|S_{21}|$ and $|S_{11}|$, respectively, for different values of ρ between 0.6 to 1.0, and L is 45 mm. The results reveal that the optimal value of ρ is 0.77.

In the case of a horn-type adapter, accurate measurement or simulation of the S -parameters is essential for achieving optimal impedance matching between the connectors and the waveguides. Impedance matching is critical for minimizing signal loss and reflection and ensuring the maximum transfer of electromagnetic energy between the two components [28].

In a WR-3.4 rectangular waveguide shown in Fig. 4 (a), the TE_{10} mode has the electric field polarized vertically. When this mode is delivered to a horn-type adapter, as shown in Fig. 4 (b), it is converted to the TE_{11} mode of the HMCW, which also has a vertical polarization, as shown in Fig. 4 (c). The simulation results of the S -parameters of the connector are shown in Fig. 4 (d). It can be seen from the results that the return losses at both ports, i.e., $|S_{11}|$ and $|S_{22}|$, are lower than 25 dB over the whole frequency range of 220-325 GHz, which indicates that the horn-type adapter provides a good impedance matching between the waveguide and the Bragg fiber. In addition, the insertion losses

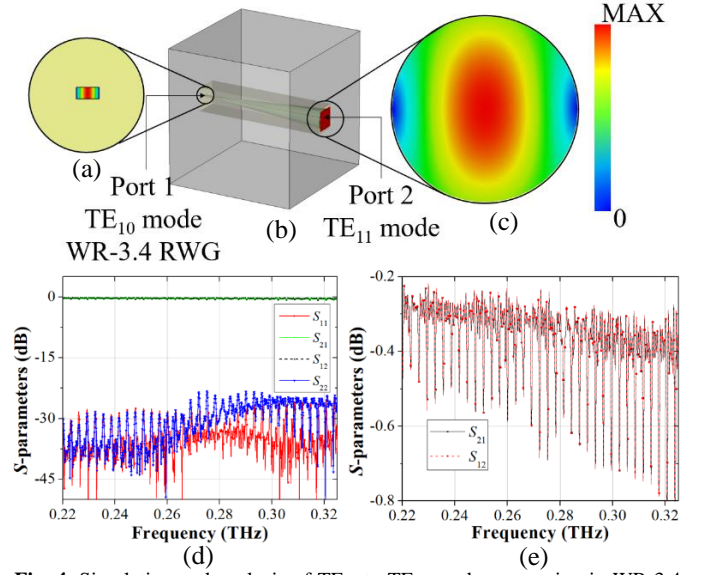


Fig. 4. Simulation and analysis of TE_{10} to TE_{11} mode conversion in WR-3.4 rectangular waveguide using horn-type adapter: S -Parameters and Reciprocity Analysis (a) The vertical polarization of TE_{10} mode at port 1 in the WR-3.4 rectangular waveguide. (b) The schematic of a horn-type adapter to convert TE_{10} mode from a WR-3.4 rectangular waveguide to TE_{11} mode in a horn-type adapter. (c) The vertical polarization of TE_{11} mode at port 2 from the horn-type adapter. (d) The CST simulation result of S -parameters at port 1 and port 2. (e) The CST simulation result of reciprocity of return loss between port 1 and port 2.

in the two directions, i.e., $|S_{21}|$ and $|S_{12}|$, are lower than 1 dB, as clearly seen in Fig. 4 (e), which exhibits an efficient coupling provided by the horn-type adapter. Fig. 4 (e) also shows that $|S_{21}|$ and $|S_{12}|$ are identical, which demonstrates that the horn-type adapter has the reciprocal property. These characteristics of the horn-type adapter are achieved by properly designing the horn to have a specific geometry that provides a uniform field amplitude over the aperture, as well as the appropriate phase relationship of the field in the waveguide and the field at the output of the horn.

III. MEASUREMENT RESULTS AND DISCUSSIONS

The multiple reflections of modes at different interfaces can lead to interferences and distortions of the signal. In the proposed measurement setup using horn-type adapter, the interferences, and distortions happen at the interfaces among the HMCW, connector, and Bragg fiber, which require proper calibration to de-embed the DUT. To address these issues, a two-tier calibration [25] technique using SSLT [29] and TRL [30] methods is employed to improve the accuracy of the S -parameter measurements. It should be noted that the L in SSLT and TRL represent different standards. In SSLT, L means Load, whereas in TRL, L means Line. The first-tier full two-port SSLT calibration, which is also called offset short calibration, uses a commercial Ceyear© AV20302 mechanical calibration kit. Here, the SSLT calibration kits contain the following standards:

> REPLACE THIS LINE WITH YOUR MANUSCRIPT ID NUMBER (DOUBLE-CLICK HERE TO EDIT) <

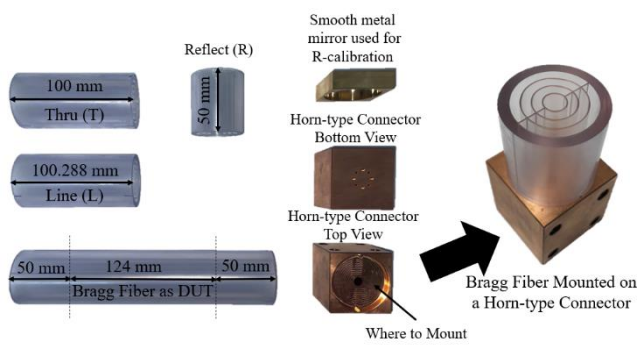


Fig. 5. Fabricated horn-type adapter and different length of the Bragg fibers for the second-tier TRL calibration technique and the fully assembled the Bragg fiber with the horn-type adapter used in this paper.

1) Short (S): A fixed flush short kit with smooth metal reflection plane is used to terminate the Bragg fiber by reflecting the signal, and hence defines the reference plane.

2) offset-Short (S): The offset-Short is made up of a quarter-wavelength straight section (shim) and an above-mentioned fixed flush short.

3) Load (L): A matched load kit with WR-3.4 rectangular waveguide aperture is used, and its return loss is greater than 25 dB.

4) Thru (T): No additional kit is required for Thru measurement, which is performed by directly connecting the two WR-3.4 rectangular waveguide of the two frequency extenders.

Following the standard calibration procedures and applying the build-in SSLT calibration algorithm in the VNA, the reference plane is moved to the end of the WR-3.4 rectangular waveguide thereafter.

Fig. 5 shows the fabricated horn-type adapters and the Bragg fibers with different lengths used in the measurement system. The second-tier TRL calibration, which includes in-situ Thru connection (T), Reflection standard (R), and Line standard (L), characterizes the performance of the component in a systematic and repeatable manner by moving the reference plane away from the joint interfaces and to a place in the Bragg fiber, to eliminate the effect of test fixtures. Here, the custom-designed TRL calibration kits used to calibrate the Bragg fiber contain the following standards:

1) Thru (T): A 100 mm length Bragg fiber is provided for thru measurement, as the reference plane is again moved to 50 mm in the Bragg fiber, away from the interface between the horn-type adaptor and the Bragg fiber.

2) Reflect (R): The reflect standard is made up of a 50 mm Bragg fiber and a smooth metal mirror. They are tightly fixed and attached to the horn-type adaptor. The place of the metal mirror determines the reference plane.

3) Line (L): The line standard is similar to the thru standard, but with an additional quarter-wavelength section in the middle. The additional quarter-wavelength section, located in the middle of the Line standard, is 3D printed and seamlessly integrated with the other sections (two 50 mm sections at the feed-in and feed-out

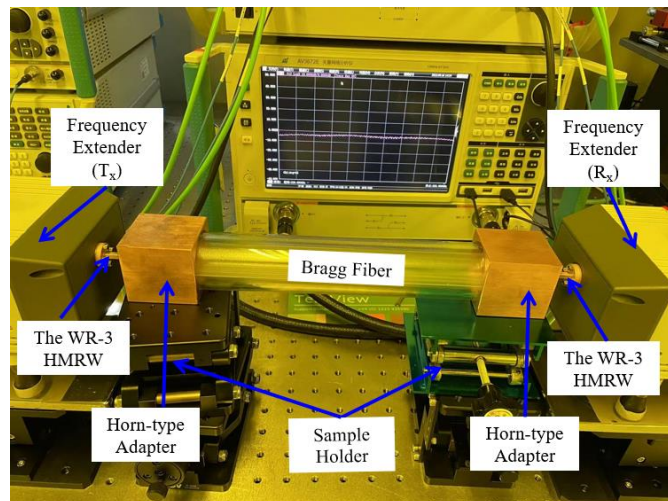


Fig. 6. The proposed measurement setup. The two horn-type adapters were attached to both open-ended sides of the WR-3.4 HMRW, and the Bragg fiber was fixed stability on the sample holders.

ports). After measuring all the second-tier calibration standards and the DUT using the VNA based on the mounting configuration shown in Fig. 6, we post-processed the acquired data with MATLAB based on Ref. [30], thereby obtaining all the S -parameters of the DUT.

By combining these methods, the two-tier calibration technique can improve the accuracy and repeatability of measurements for Bragg fiber measurement by eliminating the effect of the horn-type connector and other test fixtures, but it requires careful execution and appropriate calibration standards to minimize environmental effects.

The insertion loss (IL) is the ratio between the incident power to the transmitted power, expressed in dB, which is given by

$$IL \text{ (dB)} = -20\log|S_{21}| \quad (1)$$

where $|S_{21}|$ represents the magnitude of the transmission coefficient [31].

The return loss (RL) is the ratio of the incident power to the reflected power, expressed in dB, which is given by

$$RL \text{ (dB)} = -20\log|S_{11}| \quad (2)$$

where $|S_{11}|$ represents the magnitude of the reflection coefficient [31].

To fabricate the Bragg fiber, the design was first created using CST simulation software. The design is then loaded into the 3D Systems PolyJet 7000 HD 3D printer, and the printer is set up to print using the stereolithography technique. The next step is to fabricate the horn-type adapter using CNC milling. The connector is made of metal and is flared to match the diameter of Bragg fiber. The CNC milling machine precisely shapes and sizes the connector according to the design specifications to allow for assembly with the Bragg fiber. Finally, the performance of the THz Bragg fiber is tested using the proposed VNA-based integrated measurement setup to measure its transmission and reflection characteristics. The data

> REPLACE THIS LINE WITH YOUR MANUSCRIPT ID NUMBER (DOUBLE-CLICK HERE TO EDIT) <

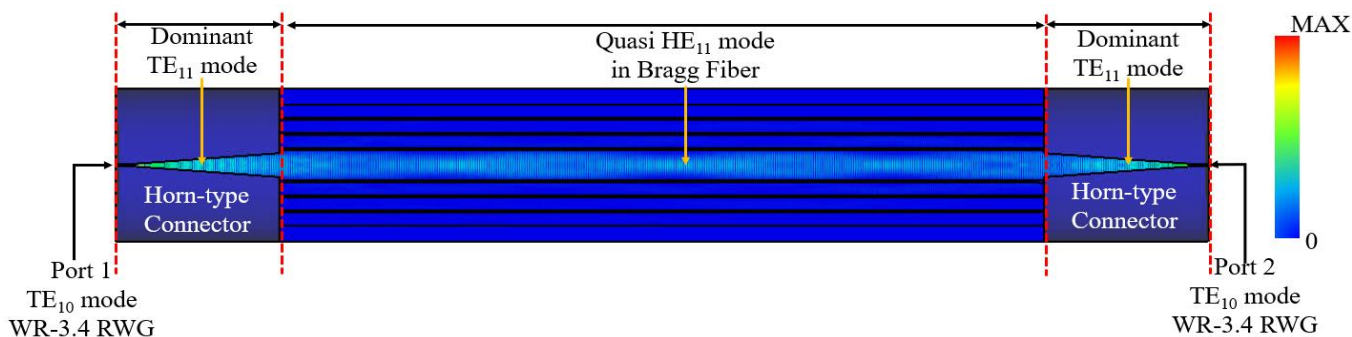


Fig. 7. The simulated electric field propagation at 265 GHz between the horn-type adapters and the Bragg fiber using a back-to-back setup.

obtained are compared with the simulation results to verify performance of the Bragg fiber.

Fig. 6 shows the measurement setup used in the study, with two horn-type adapters attached to both open-ended sides of the WR-3.4 HMRW and the Bragg fiber fixed securely on the sample holders. By using the above-mentioned two-tier calibration technique described, the Bragg fiber can be easily investigated in terms of its uncomplicated setup and repeatability. Fig. 7 shows the simulated electric field propagation at 265 GHz in a back-to-back setup between the horn-type adapters and the Bragg fiber. The simulation exhibits the TE_{10} mode, which is the fundamental mode of propagation in a WR-3.4 rectangular waveguide. However, this mode cannot efficiently couple to the Bragg fiber due to its confined electric and magnetic fields, which have a zero value at the waveguide walls. To overcome this limitation, a horn-type adapter was utilized to transform the TE_{10} mode into the dominant TE_{11} mode, which has a good beneficial field distribution for coupling. The shape of the horn gradually expands from the rectangular waveguide to a circular cross-section, allowing the wave to spread and match the impedance of the subsequent Bragg fiber.

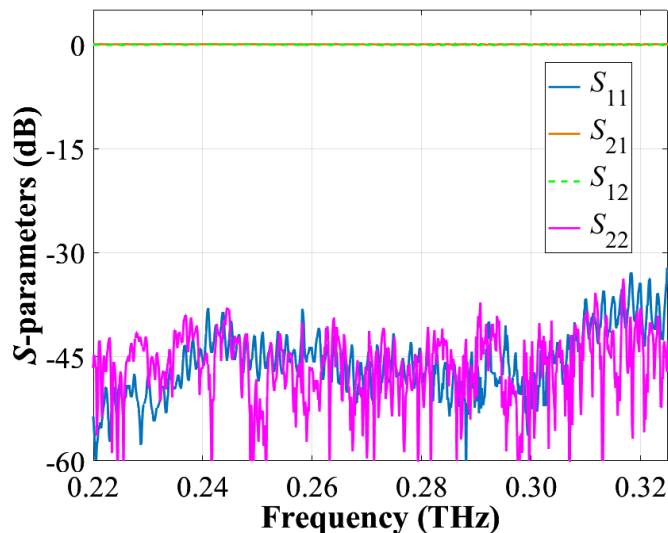


Fig.8. The measured Thru spectra with the WR-3.4 rectangular waveguides of the frequency extenders directly connected after applying the first-tier SSLT calibration

With similar mode profiles and phase velocity, the dominant TE_{11} mode in the horn-type adapter can evolve into the quasi-single- HE_{11} mode in the Bragg fiber. The Bragg fiber acts as a distributed reflector, causing multiple reflections of the electromagnetic wave, leading to the formation of a standing wave pattern. The proposed measurement setup is a VNA-based integrated setup. The key parameters of equipment used for experiments are listed in Table II. A Ceyear[®] VNA is used in this work, and the operating frequency range is extended to the range of 220-325 GHz using two frequency extenders, which are also from the Ceyear[®]. Standard WR-3.4 HMRWs are used in frequency extenders. The SSLT calibration technique was used to move the reference plane to the end of the WR-3.4 HRMW. The SSLT calibration method was utilized to ensure precise measurements of THz signals traveling through the waveguide.

TABLE II

KEY PARAMETERS OF THE EQUIPMENT USED FOR EXPERIMENTS

Equipment	Specification	Description
Vector Network Analyzer	Model	Ceyear [®] AV3672E
	Operating Frequency	10MHz – 67GHz
	Frequency Resolution	1 Hz
Frequency Extender	Waveguide	1.85 mm Coaxial Cable
	Model	Ceyear [®] AV3649A
	Operating Frequency	220GHz-320GHz
Calibration Kit	Output Waveguide	WR-3.4 Rectangular Waveguide
	Dynamic Range	≥ 100 dB @ IF=10Hz
	Model	Ceyear [®] AV20302
Calibration Kit	Type	Mechanical
	Operating Frequency	220GHz-325GHz
	Coupling Waveguide	WR-3.4 Rectangular Waveguide
	VSWR	<1.12

> REPLACE THIS LINE WITH YOUR MANUSCRIPT ID NUMBER (DOUBLE-CLICK HERE TO EDIT) <

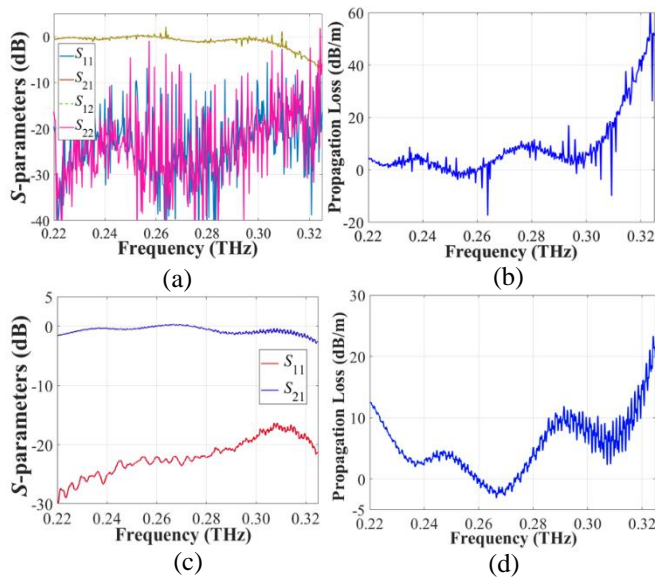


Fig. 9. Measured and simulated S -parameters and propagation loss of the Bragg fiber. (a) The measured S -parameters of the DUT. (b) The measured propagation loss of the DUT after applying the two-tier calibration technique. (c) The simulated S -parameters of the DUT. (d) The simulated propagation loss of the DUT de-embedded using the TRL calibration.

The S -parameters S_{11} and S_{21} of the Thru configuration were measured and corrected using the SSLT, as shown in Fig. 8. The S_{11} and S_{21} were found to have good performance, with S_{11} less than -40 dB and S_{21} approximately 0 dB across the frequency range of 220 GHz to 325 GHz, demonstrating the first-tier calibration is valid. Additionally, the measured Thru spectra exhibited S -parameter reciprocity [32], indicating that the calibration accurately characterized the behavior of the waveguide and removed any potential errors that can affect the measurement results.

To mitigate the effects of multiple reflections, it is important to carefully design the measurement setup and use appropriate calibration techniques. This includes the use of specialized calibration standards or techniques to account for the effects of reflections and other sources of measurement error. It is also important to carefully analyze the measurement data and perform appropriate data processing and filtering to remove any unwanted effects of multiple reflections and other sources of error. Therefore, in this study, the second-tier TRL calibration was performed to enhance the accuracy and reliability of the measurements. Fig. 9 shows the measured and simulated S -parameters and propagation loss of the Bragg fiber with a length of 124 mm. In Fig. 9 (a) and (b), the de-embedded measured insertion loss and propagation loss are less than 1.5 dB and 12 dB/m from 220 to 305 GHz. Fig. 9 (c) illustrates the de-embedded simulation results of the DUT using the proposed setup to estimate the S -parameters and propagation loss of the Bragg fiber. The return loss is less than 15 dB, and the insertion loss is less than 1.5 dB from 220 to 305 GHz. The return losses of both the measured and simulated results are relatively low, indicating that most power has been coupled into the Bragg

fiber. Fig. 9 (d) shows the simulated propagation loss of the THz Bragg fiber, which is well consistent with the measured results shown in Fig. 9 (b). There are several factors that can cause measurement results to differ slightly from simulation results. Some of the most important factors are the non-uniform dimensions of the Bragg fiber, surface roughness, and material impurities that may contribute to higher propagation losses.

Table III. shows the comparisons of key properties of the proposed VNA-based integrated setup using the two-tier calibration techniques with other existing techniques for the characterization of different types of waveguides in the THz frequency band. The table summarizes the type of waveguide, operating band, type of measurement setup, calibration technique, the complexity of setup, coupling efficiency, impedance adjustability, measurement repeatability, operator experience requirement, and cost of setup tools [33]–[42] and [43]–[47]. Three types of measurement setups are classified based on their characteristics as follows:

1) The VNA-based quasi-optical setup is very complex and requires expensive setup tools. It offers high measurement repeatability but moderate coupling efficiency and impedance matching capability. It also requires a high level of operator experience.

2) The THz-TDS-based optical setup is very complex and requires high-cost setup tools. It provides high measurement repeatability but intermediate coupling efficiency and impedance matching capability. It also requires very experienced operators.

3) The VNA-based integrated setup is less complex and requires low-cost setup tools. It offers high measurement repeatability, coupling efficiency, and impedance matching capability. In addition, it requires only a small amount of operator experience. From this comparison, the proposed VNA-based integrated setup using a horn-type adapter has more overall advantages compared to other existing measurement methods.

IV. CONCLUSION

In this paper, a novel VNA-based measurement approach for the characterization of Bragg fibers in the THz frequency range is presented. It offers high repeatability, coupling efficiency, and impedance matching capability while requiring simple setup, little operator experience, and inexpensive setup tools. The proposed method uses a horn-type adapter to efficiently couple electromagnetic waves between the test instrument and the Bragg fibers for accurate characterization. The connector was designed for the operating frequency range of 220 GHz to 325 GHz and fabricated by CNC milling technology. The suitable taper profile of the horn structure provides smooth guidance of electromagnetic waves, resulting in minimal signal loss and improved transmission efficiency. Mode matching from TE₁₁ in a horn-type adapter to HE₁₁ in a THz Bragg fiber is achieved by selecting a proper aperture size of the horn. The S -parameters were evaluated using

> REPLACE THIS LINE WITH YOUR MANUSCRIPT ID NUMBER (DOUBLE-CLICK HERE TO EDIT) <

TABLE III
COMPARISONS OF KEY PROPERTIES BETWEEN DIFFERENT THZ MEASUREMENT SETUPS.

Ref. No.	Type	Operating Band (THz)	Type of Measurement setup	Calibration technique	Complexity of setup	Coupling efficiency	Impedance adjustability	Measurement repeatability	Operator experience requirement	Cost of setup tools
[33]	Bragg fiber	0.246 – 0.276	VNA-based quasi-optical setup	Two-tier calibration: LRL calibration + cut-back calibration	Easy	Medium	Medium	Repeatable	High	High
[34]	Polymer Anti-resonant hollow core Waveguide	0.32	THz-TDS optical setup	Normalization	Hard	Medium	Medium	Repeatable	High	High
[35]	Anti-resonant hollow core fiber	0.6	THz-TDS optical setup	Cut-back	Hard	Medium	Medium	Repeatable	High	High
[36]	Anti-resonant Hollow core fiber	2.15	THz-TDS optical setup	Cut-back	Hard	Medium	Medium	Repeatable	High	High
[37]	TOPAS Suspended core-microstructured polymer optical fiber (TOPAS SC-MPOF)	0.5-1.0	THz-TDS optical setup	Cut-back	Hard	Medium	Medium	Repeatable	High	High
[38]	Anti-resonant Hollow core fiber	0.29	THz-TDS optical setup	Cut-back	Hard	Medium	Medium	Repeatable	High	High
[39]	Bragg waveguide	0.158-0.202	THz-CW and THz-TDS optical setup	Cut-back	Hard	Medium	Medium	Repeatable	High	High
[40]	Kagome	0.25	THz-TDS optical setup	Cut-back	Hard	Medium	Medium	Repeatable	High	High
[41]	photonic-crystal waveguides	0.3	THz-CW optical setup	Cut-back	Hard	Medium	Medium	Repeatable	High	High
[42]	Photonic crystal waveguides	0.33	THz-CW optical setup	Cut-back	Hard	Medium	Medium	Repeatable	High	High
[43]	Bragg fiber	0.35	THz-TDS optical setup	Normalization	Hard	Medium	Medium	Repeatable	High	High
[44]	Anti-resonant Hollow core fiber	0.24	THz-TDS optical setup	Normalization	Hard	Medium	Medium	Repeatable	High	High
[45]	Suspended core microstructured fiber	0.128	THz-CW optical setup	Cut-back	Hard	Medium	Medium	Repeatable	High	High
[46]	MPOF Porous Core	0.39-0.45	THz-TDS optical setup	Cut-back	Hard	Medium	Medium	Repeatable	High	High
[47]	Pentagram THz Hollow Core Anti-resonant Fiber (HC-ARF)	1	THz-TDS optical setup	Cut-back	Hard	Medium	Medium	Repeatable	High	High
This work	Bragg fiber	0.22-0.325	VNA-based integrated setup	Two-tier Calibration	Easy	High	High	Highly Repeatable	Low	Low

> REPLACE THIS LINE WITH YOUR MANUSCRIPT ID NUMBER (DOUBLE-CLICK HERE TO EDIT) <

the two-tier calibrations, SSLT and TRL, to eliminate sources of error and ensure reliable, consistent, and robust measurements. The performance of the horn-type-connector shows that the return loss is less than 25 dB, and the insertion loss is nearly zero, indicating good signal transmission efficiency and minimal signal loss and reflection. Moreover, the de-embedded simulation and measurement results of the DUT using the proposed setup also show the accuracy of the S -parameters and propagation loss of the Bragg fiber. The measured return loss of the DUT is about 15 dB, and the propagation loss is about 12 dB/m, which agrees well with the simulated results.

ACKNOWLEDGMENT

The authors would like to thank N. Duangrit at the National Astronomical Research Institute of Thailand for his advice on microstructured measurements and evaluations. B. Hong and R. Viratikul equally contribute to all works completed in this paper.

REFERENCES

- [1] G. Gallerano and S. Biedron, "Overview of terahertz radiation sources," *Proc. 2004 FEL Conf.*, pp. 216–221, 2004.
- [2] N. Chudpooti, P. Sangpet, S. Chudpooti, P. Akkaraekthalin, I. D. Robertson, and N. Somjit, "An Incorporated 3D-Printed Lens with Square Microstrip Patch Antenna for NaCl Solution Discrimination," *Proc. - 2022 Res. Invent. Innov. Congr. Innov. Electr. Electron. RI2C 2022*, pp. 259–262, 2022, doi: 10.1109/RI2C56397.2022.9910338.
- [3] N. Chudpooti, N. Duangrit, S. Chudpooti, P. Akkaraekthalin, I. D. Robertson, and N. Somjit, "THz Photo-Polymeric Lens Antennas for Potential 6G Beamsteering Frontend," *2021 Int. Symp. Antennas Propagation, ISAP 2021*, pp. 15–16, 2021, doi: 10.23919/ISAP47258.2021.9614562.
- [4] S. Atakaramians, S. Afshar V., T. M. Monro, and D. Abbott, "Terahertz dielectric waveguides," *Adv. Opt. Photonics*, vol. 5, no. 2, p. 169, 2013, doi: 10.1364/aop.5.000169.
- [5] T. Nagatsuma, "Terahertz technologies: Present and future," *IEICE Electron. Express*, vol. 8, no. 14, pp. 1127–1142, 2011, doi: 10.1587/elex.8.1127.
- [6] M. Islam, D. R. Chowdhury, A. Ahmad, and G. Kumar, "Terahertz Plasmonic Waveguide Based Thin Film Sensor," *J. Light. Technol.*, vol. 35, no. 23, pp. 5215–5221, 2017, doi: 10.1109/JLT.2017.2763326.
- [7] S. Chudpooti, P. Sangpet, N. Chudpooti, N. Sathitanon, N. Somjit, and P. Akkaraekthalin, "A Square Patch Partially Reflective Surface for Improving the Antenna Gain Characteristic of Low-Cost Dual Polarized Microstrip Antenna," *Proc. - 2022 Res. Invent. Innov. Congr. Innov. Electr. Electron. RI2C 2022*, pp. 255–258, 2022, doi: 10.1109/RI2C56397.2022.9910284.
- [8] B. Hong *et al.*, "Five-channel frequency-division multiplexing using low-loss epsilon-near-zero metamaterial waveguide," *Sci. China Physics, Mech. Astron.*, vol. 65, no. 7, 2022, doi: 10.1007/s11433-021-1901-0.
- [9] N. Duangrit, B. Hong, A. D. Burnett, P. Akkaraekthalin, I. D. Robertson, and N. Somjit, "Terahertz Dielectric Property Characterization of Photopolymers for Additive Manufacturing," *IEEE Access*, vol. 7, pp. 12339–12347, 2019, doi: 10.1109/ACCESS.2019.2893196.
- [10] R. T. Ako, A. Upadhyay, W. Withayachumnankul, M. Bhaskaran, and S. Sriram, "Dielectrics for Terahertz Metasurfaces: Material Selection and Fabrication Techniques," *Adv. Opt. Mater.*, vol. 8, no. 3, 2020, doi: 10.1002/adom.201900750.
- [11] K. Boonlom *et al.*, "Active Pre-Equalizer for Broadband Optical Wireless Communication Integrated with RF Amplifier," *Proc. - 2022 Res. Invent. Innov. Congr. Innov. Electr. Electron. RI2C 2022*, pp. 251–254, 2022, doi: 10.1109/RI2C56397.2022.9910315.
- [12] M. Uthman, B. M. A. Rahman, N. Kejalakshmy, A. Agrawal, and K. T. V. Grattan, "Design and characterization of low-loss porous-core photonic crystal fiber," *IEEE Photonics J.*, vol. 4, no. 6, pp. 2315–2325, 2012, doi: 10.1109/JPHOT.2012.2231939.
- [13] F. A. Mou, M. M. Rahman, M. A. Al Mahmud, M. R. Islam, and M. I. H. Bhuiyan, "Design and Characterization of a Low Loss Polarization Maintaining Photonic Crystal Fiber for THz Regime," *3rd IEEE Int. Conf. Telecommun. Photonics, ICTP 2019*, pp. 3–6, 2019, doi: 10.1109/ICTP48844.2019.9041715.
- [14] B. Hong, N. Somjit, J. Cunningham, and I. Robertson, "Design study of low loss single-mode hollow core photonic crystal terahertz waveguide with support bridges," *IRMMW-THz 2015 - 40th Int. Conf. Infrared, Millimeter, Terahertz Waves*, pp. 15–16, 2015, doi: 10.1109/IRMMW-THz.2015.7327404.
- [15] O. Mitrofanov, R. James, F. A. Fernández, T. K. Mavrogordatos, and J. A. Harrington, "in Hollow THz Waveguides," *Science (80-)*, vol. 1, no. 1, pp. 124–132, 2011.
- [16] B. Hong, Y. Qiu, N. Somjit, J. Cunningham, I. Robertson, and G. P. Wang, "Guidance of Terahertz Wave over Commercial Optical Fiber," *Int. Conf. Infrared, Millimeter, Terahertz Waves, IRMMW-THz*, vol. 2021-Augus, pp. 3–4, 2021, doi: 10.1109/IRMMW-THz50926.2021.9566906.
- [17] N. Chudpooti, N. Duangrit, P. Akkaraekthalin, I. D. Robertson, and N. Somjit, "Terahertz Free-Space Measurement System Using Low-Cost 3D-Printed Hemispherical Lens Antenna," *Proc. - 2021 Res. Invent. Innov. Congr. Innov. Electr. Electron. RI2C 2021*, pp. 110–114, 2021, doi: 10.1109/RI2C51727.2021.9559829.
- [18] C. Caglayan, G. C. Trichopoulos, and K. Sertel, "Non-contact probes for on-wafer characterization of sub-millimeter-wave devices and integrated circuits," *IEEE Trans. Microw. Theory Tech.*, vol. 62, no. 11, pp. 2791–2801, 2014, doi: 10.1109/TMTT.2014.2356176.
- [19] D. Helena, A. Ramos, T. Varum, and J. N. Matos, "The use of 3d printing technology for manufacturing metal antennas in the 5g/iot context," *Sensors*, vol. 21, no. 10, 2021, doi: 10.3390/s21103321.
- [20] Y. Yang *et al.*, "Designing a water-immersed rectangular horn antenna for generating underwater OAM Waves," *Electron.*, vol. 8, no. 11, 2019, doi: 10.3390/electronics8111224.
- [21] B. Zhang, Y. X. Guo, H. Sun, and Y. Wu, "Metallic, 3D-Printed, K-band-stepped, double-ridged square horn antennas," *Appl. Sci.*, vol. 8, no. 1, 2017, doi: 10.3390/app8010033.
- [22] R. Viratikul *et al.*, "Electromagnetic Property Characterization and Sensing of Endothelial Cells Growth Medium and Dulbecco's Phosphate Buffered Saline Solution for in vitro Cell Culture," *19th Int. Conf. Electr. Eng. Comput. Telecommun. Inf. Technol. ECTI-CON 2022*, pp. 1–4, 2022, doi: 10.1109/ECTI-CON54298.2022.9795438.
- [23] S. L. Rumyantsev *et al.*, "Terahertz Beam Testing of Millimeter Wave Monolithic Integrated Circuits," *IEEE Sens. J.*, vol. 17, no. 17, pp. 5487–5491, 2017, doi: 10.1109/JSEN.2017.2725744.
- [24] B. Hong, M. Swithenbank, N. Somjit, J. Cunningham, and I. Robertson, "Asymptotically single-mode small-core terahertz Bragg fibre with low loss and low dispersion," *J. Phys. D. Appl. Phys.*, vol. 50, no. 4, 2017, doi: 10.1088/1361-6463/aa519d.
- [25] S. Lucyszyn, "Measurement techniques," in *RFIC and MMIC Design and Technology*, I. D. Robertson and S. Lucyszyn, eds., London, U.K.: IET,

> REPLACE THIS LINE WITH YOUR MANUSCRIPT ID NUMBER (DOUBLE-CLICK HERE TO EDIT) <

- 2001, ch. 12, sec. 2, pp. 514–523.
- [26] B. Hong, N. Chudpooti, P. Akkarakthalin, N. Somjit, J. Cunningham, and I. Robertson, “Investigation of electromagnetic mode transition and filtering of an asymptotically single-mode hollow THz Bragg fibre,” *J. Phys. D: Appl. Phys.*, vol. 51, no. 30, 2018, doi: 10.1088/1361-6463/aaccaa.
- [27] B. Hong *et al.*, “Substrate integrated Bragg waveguide: an octave-bandwidth single-mode hybrid transmission line for millimeter-wave applications,” *Opt. Express*, vol. 28, no. 19, p. 27903, 2020, doi: 10.1364/oe.399160.
- [28] W. Fu *et al.*, “Polarization insensitive wide-angle triple-band metamaterial bandpass filter,” *J. Phys. D: Appl. Phys.*, vol. 49, no. 28, 2016, doi: 10.1088/0022-3727/49/28/285110.
- [29] W. Luo, A. Hu, K. Liu, and X. Chen, “Study on SLT calibration method of 2-port waveguide DUT,” *International Conference on Advanced Electronic Science and Technology*, pp. 276–282, 2016, doi: 10.2991/aest-16.2016.37.
- [30] A. I. Technique and N. Analyzer, ““Thru-Reflect-Line”: An Improved Technique for Calibrating the Dual Six-Port Automatic Network Analyzer,” *Technology*, pp. 987-993, 1979, doi: 10.1109/TMTT.1979.1129778
- [31] N. C. Das, T. K. Chaki, D. Khastgir, and A. Chakraborty, “Electromagnetic interference shielding effectiveness of conductive carbon black and carbon fiber-filled composites based on rubber and rubber blends,” *Adv. Polym. Technol.*, vol. 20, no. 3, pp. 226–236, 2001, doi: 10.1002/adv.1018.
- [32] U. Stumper, “Influence of nonideal calibration items on S-parameter uncertainties applying the SOLR calibration method,” *IEEE Trans. Instrum. Meas.*, vol. 58, no. 4, pp. 1158–1163, 2009, doi: 10.1109/TIM.2008.2006962.
- [33] B. Hong *et al.*, “Low-Loss Asymptotically Single-Mode THz Bragg Fiber Fabricated by Digital Light Processing Rapid Prototyping,” *IEEE Trans. Terahertz Sci. Technol.*, vol. 8, no. 1, pp. 90–99, 2018, doi: 10.1109/TTHZ.2017.2778047.
- [34] L. D. van Putten, J. Gorecki, E. Numkam Fokoua, V. Apostolopoulos, and F. Poletti, “3D-printed polymer antiresonant waveguides for short-reach terahertz applications,” *Appl. Opt.*, vol. 57, no. 14, p. 3953, 2018, doi: 10.1364/ao.57.003953.
- [35] S. Yang, X. Sheng, G. Zhao, S. Lou, and J. Guo, “3D Printed Effective Single-Mode Terahertz Antiresonant Hollow Core Fiber,” *IEEE Access*, vol. 9, pp. 29599–29608, 2021, doi: 10.1109/ACCESS.2021.3059782.
- [36] M. M. Nazarov *et al.*, “Eight-Capillary Cladding THz Waveguide with Low Propagation Losses and Dispersion,” *IEEE Trans. Terahertz Sci. Technol.*, vol. 8, no. 2, pp. 183–191, 2018, doi: 10.1109/TTHZ.2017.2786030.
- [37] T. Wanvisa *et al.*, “Singlemoded THz guidance in bendable TOP AS suspended-core fiber directly drawn from a 3D printer,” *Nature*, 2020, doi: 10.1038/s41598-020-68079-y.
- [38] S. Yang, X. Sheng, G. Zhao, S. Lou, and J. Guo, “Anti-deformation low loss double pentagon nested terahertz hollow core fiber,” *Opt. Fiber Technol.*, vol. 56, no. March, 2020, doi: 10.1016/j.yofte.2020.102199.
- [39] J. Li, K. Nallapan, H. Guerboukha, and M. Skorobogatiy, “3D printed hollow core terahertz Bragg waveguide for surface sensing applications,” *2017 Conf. Lasers Electro-Optics, CLEO 2017 - Proc.*, vol. 2017-Janua, no. 4, pp. 1–2, 2017, doi: 10.1364/CLEO_AT.2017.JW2A.101.
- [40] J. Yang *et al.*, “3D printed low-loss THz waveguide based on Kagome photonic crystal structure,” *Opt. Express*, vol. 24, no. 20, p. 22454, 2016, doi: 10.1364/oe.24.022454.
- [41] X. Yu *et al.*, “Terahertz fibre transmission link using resonant tunnelling diodes integrated with photonic-crystal waveguides,” *Electron. Lett.*, vol. 55, no. 7, pp. 398–400, 2019, doi: 10.1049/el.2018.7686.
- [42] K. Tsuruda, M. Fujita, and T. Nagatsuma, “Extremely low-loss terahertz waveguide based on silicon photonic-crystal slab,” *Opt. Express*, vol. 23, no. 25, p. 31977, 2015, doi: 10.1364/oe.23.031977.
- [43] A. L. S. Cruz, A. Argyros, X. Tang, C. M. B. Cordeiro, and M. A. R. Franco, “3D-printed terahertz Bragg fiber,” *IRMMW-THz 2015 - 40th Int. Conf. Infrared, Millimeter, Terahertz Waves*, pp. 5–6, 2015, doi: 10.1109/IRMMW-THz.2015.7327936.
- [44] A. L. S. Cruz *et al.*, “3D printed hollow core fiber with negative curvature for terahertz applications,” *J. Microwaves, Optoelectron. Electromagn. Appl.*, vol. 14, no. February 2016, pp. SI45–SI53, 2015.
- [45] G. Xu, K. Nallapan, Y. Cao, and M. Skorobogatiy, “Infinity additive manufacturing of continuous microstructured fiber links for THz communications,” *Sci. Rep.*, vol. 12, no. 1, pp. 1–13, 2022, doi: 10.1038/s41598-022-08334-6.
- [46] S. Mei *et al.*, “A porous core Zeonex THz fiber with low loss and small dispersion,” *Opt. Fiber Technol.*, vol. 69, no. October 2021, 2022, doi: 10.1016/j.yofte.2022.102834.
- [47] S. Yang, X. Sheng, G. Zhao, Y. Wang, and Y. Yu, “Novel Pentagon THz Hollow Core Anti-resonant Fiber Using a 3D Printer,” *J. Infrared, Millimeter, Terahertz Waves*, vol. 40, no. 7, pp. 720–730, 2019, doi: 10.1007/s10762-019-00600-5.